Review | Received 14 August 2025; Revised 22 October 2025; Accepted 28 October 2025; Published 12 November 2025
https://doi.org/10.55092/opr20250001

Nanoimprint lithography for scalable manufacturing of optical metasurfaces

Yujin Park[1,†], **Donghoe Kim**[1,†] **and Junsuk Rho**[1,2,3,4,*]

[1] Department of Mechanical Engineering, Pohang University of Science and Technology (POSTECH), Pohang 37673, Republic of Korea
[2] Department of Chemical Engineering, Pohang University of Science and Technology (POSTECH), Pohang 37673, Republic of Korea
[3] Department of Electrical Engineering, Pohang University of Science and Technology (POSTECH), Pohang 37673, Republic of Korea
[4] POSCO-POSCTECH-RIST Convergence Research Center for Flat Optics and Metaphotonics, Pohang 37673, Republic of Korea

† These authors contributed equally to this work.

* Correspondence author; E-mail: jsrho@postech.ac.kr.

Highlights:

- Nanoimprint lithography (NIL) is reviewed as a promising technique for the low-cost and large-scale fabrication of metasurfaces.
- Hybrid materials and particle-embedded resin (PER) processes are analyzed to overcome the low refractive index limitation of conventional NIL resin.
- PER-based metasurfaces are demonstrated to operate across ultraviolet (UV), visible, and infrared (IR) wavelength ranges, and can be applied to curved (LiDAR) and biodegradable (food label) substrates.

Abstract: Metasurfaces, composed of two-dimensional meta-atoms with subwavelength dimensions, enable precise manipulation of light wavefronts, facilitating lensing, color filtering, holography, and augmented reality in a compact form factor. To realize desired optical functionalities, metasurface fabrication requires nanoscale patterning of high-refractive-index (high-index) materials. Conventionally, electron beam lithography (EBL) has been widely utilized in combination with deposition techniques such as plasma-enhanced chemical vapor deposition. Despite offering high-resolution capabilities, EBL suffers from low throughput, high cost, and limited scalability due to its direct-writing nature. To overcome these limitations, nanoimprint lithography (NIL) has emerged as a promising low-cost, high-throughput alternative. However, conventional NIL resins have low refractive indices (~1.5), restricting their direct optical use and necessitating additional steps to enhance the refractive index. To address this challenge, we review two strategies for the scalable fabrication of metasurfaces: hybrid materials, which apply high-index atomic layer deposition (ALD) coatings onto imprinted patterns, and particle-embedded

Copyright©2025 by the authors. Published by ELSP. This work is licensed under Creative Commons Attribution 4.0 International License, which permits unrestricted use, distribution, and reproduction in any medium provided the original work is properly cited.

resins (PERs), which incorporate high-index nanoparticles directly into the imprint resin. This review highlights recent progress in these NIL-based approaches and discusses their potential to bridge the gap between laboratory-scale demonstrations and large-scale industrial production of metasurfaces.

Keywords: nanoimprint lithography; metasurface; commercialization of metasurfaces; metaphotonics; manufacturing platform; high refractive index

1. Introduction

Metasurfaces, composed of subwavelength-scale meta-atoms, offer precise control over the light wavefront, including amplitude, phase, and polarization. Owing to their compact form factor compared to conventional bulky optical components, they have been widely adopted in diverse applications such as holography [1–9] and color filtering [10–17]. They play a crucial role in the development of compact and high-performance optical systems, being extensively utilized in metalenses [18–27] and augmented reality (AR) devices [28–31]. More recently, metasurfaces have demonstrated remarkable versatility, enabling integration with diverse fields and opening new opportunities for advanced optical platforms such as biosensing [32–35] and other emerging photonic technologies [36–43]. To enable such functionalities, the fabrication of metasurfaces typically requires nanoscale patterning of high-refractive-index (high-index) materials. Electron beam lithography (EBL), which benefits from the extremely short de Broglie wavelength of electrons, provides virtually diffraction-free patterning with resolutions down to ~80 nm. Consequently, a common fabrication route involves depositing high-index materials via plasma-enhanced chemical vapor deposition (PECVD), followed by EBL patterning. However, the direct-write nature of EBL imposes inherent limitations in terms of scalability, due to its high cost, low throughput, and slow processing speed. To overcome these challenges and bridge the lab-to-industry gap, significant efforts have been devoted to alternative fabrication strategies.

As a promising alternative, nanoimprint lithography (NIL) has emerged as a high-throughput fabrication technique [44–50]. By using a soft mold similar to a stamp, NIL enables the repeated replication of nanostructures once the initial master mold is created, offering a cost-effective and rapid production process [51–54]. This makes NIL particularly attractive for the commercialization of metasurfaces. However, conventional imprint resins typically have a low refractive index (~1.5), which limits their direct use in optical applications. As a result, NIL has primarily been employed as an etching mask to transfer patterns into underlying high-index materials rather than serving as the functional metasurface itself. Therefore, the integration of NIL into the fabrication of metasurfaces directly has been long studied.

To overcome these limitations, two primary strategies have been developed to enhance the effective refractive index (effective index) of imprint resins. These approaches enable the direct use of NIL for high-performance metasurface fabrication. The first strategy involves the use of hybrid materials, in which a high-index thin film is conformally deposited onto the imprinted metasurface via atomic layer deposition (ALD). In this approach, a metasurface is first patterned in a low-refractive-index (low-index) resin using NIL, followed by a conformal ALD coating of materials such as TiO_2 (for visible wavelengths) or ZrO_2 (for ultraviolet (UV) wavelengths). This conformal coating increases the effective index of the resulting nanostructures and significantly improves their optical performance. An

alternative strategy incorporates high-index nanoparticles directly into the imprint resin. These nanoparticle-embedded resins (PER) can be cured by UV exposure, initiating a photopolymerization reaction for rapid crosslinking [55–63]. Alternatively, they can be also cured through thermal annealing to promote solidification [64–66]. This one-step PER-based NIL (PER-NIL) process enables direct patterning of functional optical metasurfaces without any additional process.

In this review, we aim to introduce NIL-based fabrication lithography as a scalable, cost effective, and highly efficient approach compared with other lithography techniques (Table 1). To emphasize the benefits of NIL-based methods, this review is organized into three chapters outlining the progress of metasurface fabrication. In the first chapter, conventional methods using EBL and PECVD are briefly introduced. Subsequently, Chapter 2 describes traditional NIL method as an alternative to conventional EBL approaches and explains its limitation arising from the low-index commercial imprint resins. Chapter 3, the main part of this review, presents NIL-based scalable fabrication methods. This chapter is further divided into three sections: hybrid materials, PER, and the applications of PER methods.

Table 1. Comparison of various nanopatterning methods in terms of throughput, process complexity, cost, and optical efficiency.

Patterning Methods	Throughput	Cost	General Procedure	Efficiency
EBL + PECVD [67]	Very low	Very high	1. High-index film deposition 2. E-beam exposure 3. Hard mask deposition 4. Etching	Very high
DUV Lithography [68]	High	Very high	1. Photomask preparation 2. High-index film deposition 3. DUV exposure 4. Hard mask deposition 5. Etching	Very high
Nano transfer printing [69]	Medium	Medium	1. Mold preparation 2. Material deposition onto mold 3. Pattern transfer	High
NIL [70]	Very high	Low	1. Mold preparation 2. Pattern transfer	Low
PER-NIL [65]	Very high	Low	1. Mold preparation 2. Pattern transfer	High

2. Results

2.1. Conventional fabrication methods for metasurfaces

The fabrication of metasurfaces requires two key elements: high-resolution patterning and the use of high-index materials. In order to fulfill these requirements, this chapter provides an overview of the conventional metasurface fabrication process based on EBL and PECVD.

2.1.1. Electron beam lithography and plasma-enhanced chemical vapor deposition

To pattern high-resolution nanostructures, EBL is particularly advantageous due to the extremely short de Broglie wavelength of electrons, which overcomes the diffraction limit inherent to optical lithography. EBL enables direct writing using a tightly focused electron beam with a sub-nanometer

spot size, allowing for the definition of features well below 100 nm. On the other hand, to implement high-index materials, PECVD is commonly employed to deposit thin films with desirable optical properties. These films can then be patterned via EBL, combining material performance with nanoscale resolution for metasurface fabrication. The representative fabrication process for metasurface is shown in Figure 1a. The process begins with the deposition of a high-index material onto the substrate, followed by spin-coating a photoresist layer on top. The nanopatterns are defined in the photoresist layer using EBL. The exposed patterns are then developed in developer at 0 °C for approximately 12 minutes. A chromium (Cr) layer is subsequently deposited to serve as a hard mask for etching. Finally, plasma etching is employed to vertically transfer the patterns into the high-index material, forming the meta-atoms.

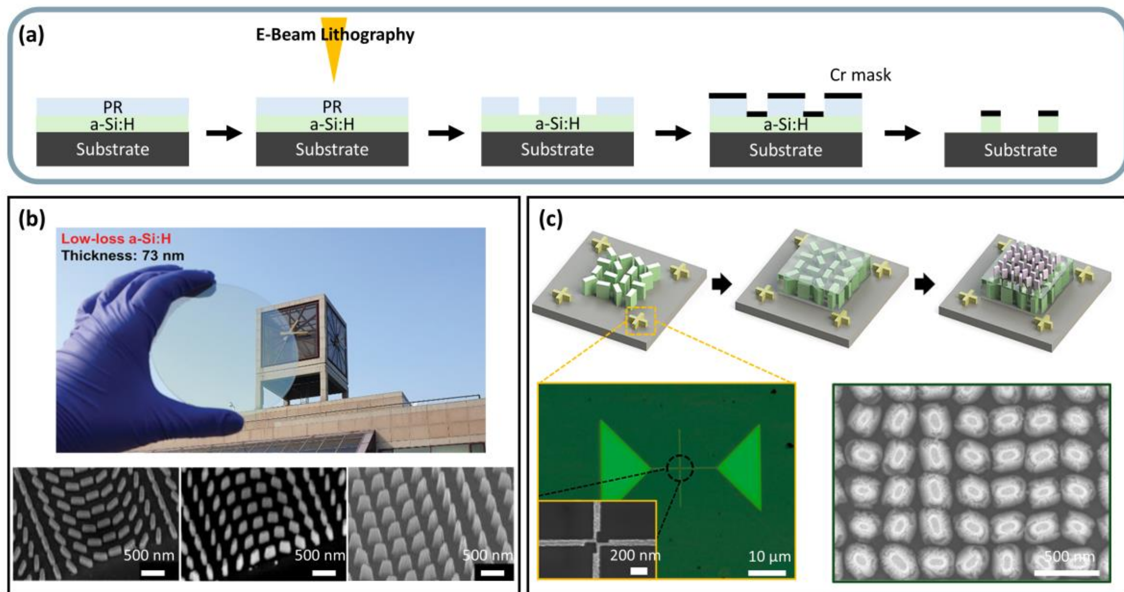

Figure 1. Conventional approach to metasurface fabrication. **(a)** Representative fabrication flow of metasurfaces employing plasma-enhanced chemical vapor deposition (PECVD) and electron beam lithography (EBL) techniques; **(b)** Demonstration of visible range (365–635 nm) beam-deflector metasurfaces fabricated with reduced extinction coefficients through optimized PECVD conditions. Scanning electron microscope (SEM) images show representative metasurfaces designed for 365, 532, and 635 nm operation [67]. Reprinted with permission. Copyright 2021 John Wiley and Sons; **(c)** Multilayer metasurface fabrication enabled by EBL overlay lithography, demonstrating a dual-band vectorial metahologram operating at an ultraviolet (UV) wavelength of 325 nm and a visible wavelength of 532 nm [1]. Reprinted with permission. Copyright 2022 American Chemical Society.

As a demonstration, the fabrication of low-loss silicon metasurfaces using EBL and PECVD is demonstrated as illustrated in Figure 1b [67]. The metasurfaces are designed to operate as beam deflectors across the visible spectrum (365–635 nm). In this process, hydrogenated amorphous silicon (a-Si:H) is used as the material, and the PECVD parameters, such as temperature, pressure, and gas mixture are optimized to minimize material's optical loss. This optimization significantly reduces the extinction coefficient (k), which is critical for enhancing conversion efficiency in metasurfaces. As a result, the fabricated metasurfaces exhibit high deflection efficiency up to 75% and clear beam deflection angles of 9.9°, 12.7°, and 11.3° for wavelengths of 450 nm, 532 nm, and 635 nm, respectively. They

provide a platform for fabricating low-loss metasurfaces and, in combination with EBL, demonstrate its potential for dielectric metasurfaces operating in the visible range.

With the growing interest in high degree-of-freedom metasurfaces, overlay techniques in EBL have been actively explored by various research groups. By employing alignment markers, layer-by-layer fabrication becomes feasible, enabling the precise registration of a second layer onto the first with an alignment accuracy of 20 nm [1]. This multilayer approach allows for the stacking of different materials, as well as the integration of features with varying heights and lateral dimensions, thereby expanding the design freedom and functionality of metasurfaces. As a representative demonstration of the EBL overlay method, multilayer dual-band vectorial metahologram is reported operating in both UV (325 nm) and visible (532 nm) spectral regions (Figure 1c). This device is realized by sequentially stacking two independently designed metasurfaces, each optimized for a specific wavelength band. Using alignment markers and high-precision stage control, dual-band metasurface is successfully fabricated. The overlay process begins with the fabrication of a visible-band metasurface using silicon nitride (SiN_x) deposited by PECVD, followed by spin coating of a 100 nm-thick spin-on-glass (SOG) silica spacer layer. The UV-band metasurface is then aligned and patterned atop the spacer layer using EBL. Optically, each metasurface layer is engineered to exhibit high cross-polarization efficiency at its target wavelength while remaining largely inactive at the other wavelength. The UV meta-atom ($meta_{325}$) shows high cross-polarization and low co-polarization efficiency at 325 nm, but low cross-polarization and high co-polarization efficiency at 532 nm. Conversely, the visible meta-atom ($meta_{532}$) maintains high cross-polarization efficiency at 532 nm while exhibiting low efficiency in the UV range. This approach allows for the integration of multiple vectorial holograms encoded in different spectral bands, with the UV metasurface achieving a conversion efficiency of 72% and 17.9% at 325 and 532 nm, respectively. The successful realization of metasurface with dual-band operation underscores the potential of EBL overlay lithography for complex, high-capacity metasurface platforms.

2.2. Conventional nanoimprint lithography

EBL offers high resolution [71,72] and compatibility with high-index materials [73]. While it also provides suitability for overlay processes [74–78], its serial, direct-writing nature inherently limits throughput, resulting in high cost and slow processing speed. As interest in the commercialization of metasurfaces continues to grow, the demand for alternative fabrication methods to overcome these limitations has emerged. Accordingly, this chapter introduces NIL as a scalable, low cost, and high throughput lithography technique.

2.2.1. Nanoimprint lithography with low-refractive-index resin

NIL has emerged as a promising lithographic approach, combining low cost, high throughput, and versatile patterning capabilities. Depending on the resin curing mechanism, NIL is typically divided into thermal NIL and UV-NIL. In thermal NIL, a thermoplastic resist is patterned and solidified through heating, whereas in UV-NIL, a UV-curable resist is crosslinked upon UV irradiation [79]. The thermal NIL process generally proceeds through the following steps (Figure 2a) [70]. First, the thermoplastic resist is heated above its glass transition temperature (T_g), where it transitions into a rubbery, deformable state. A mold is then pressed into the softened resist to replicate the nanoscale features. Once imprinting

is complete, the system is cooled below T_g, solidifying the resist. Throughout the cooling phase, pressure is maintained to preserve pattern fidelity. Finally, the mold is separated from the solidified resist, leaving the imprinted nanostructures [45]. By leveraging this mechanism, Chou *et al.* demonstrate the fabrication of dot arrays with diameters of 25 nm and trenches with widths of 60 nm and depths of 100 nm [44]. They utilize polymethyl methacrylate (PMMA) as a thermoplastic resist; the PMMA layer and the mold are both heated to 200 °C, exceeding the T_g of 105 °C, and pressed under a pressure of approximately 13.1 MPa.

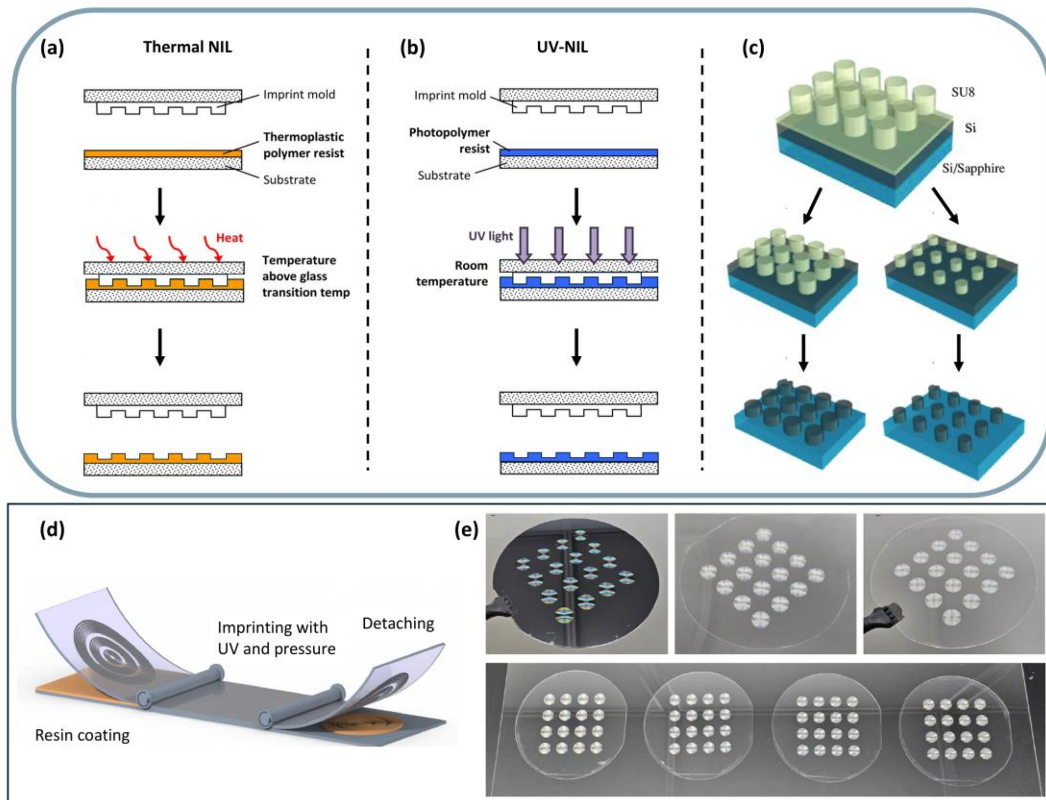

Figure 2. Schematic diagrams of the conventional nanoimprint lithography (NIL) process. **(a, b)** The schematic illustration of the overall fabrication processes of thermal NIL and UV-NIL, respectively [70]; **(c)** The process schematic showing the use of SU-8 photoresist as an etching mask. The size of the etching mask decreases with etching time, resulting in variations in the structure size [80]; **(d)** Schematic illustration of roll-to-plate (R2P) process for fabricating achromatic metalenses; **(e)** Photographs of the master mold, replica mold, and fabricated metalenses, along with large-scale fabrication results [81].

In contrast, UV-NIL has emerged as a promising alternative to thermal NIL, overcoming limitations such as time-consuming thermal cycles and pattern distortion caused by the thermal expansion mismatch between the mold and the substrate. It utilizes low-viscosity photoresists composed of photocurable monomers and a photo-initiator. The typical UV-NIL process begins with the preparation of high-resolution master molds (Figure 2b) [70]. A low-viscosity, spin-coatable UV-curable resin is then uniformly deposited onto the substrate. Then, the mold is aligned and brought into contact with the coated substrate. UV light is subsequently applied to initiate a photopolymerization reaction, resulting in rapid curing of the resin. Once the curing is complete, the mold is separated from the substrate, leaving the

imprinted structures on the substrate. A residual layer is inherently formed on the substrate during the imprinting process, but it can be effectively removed by plasma etching after the imprint step is completed. For a successful UV-NIL process, the properties of the UV-curable resin must be carefully selected based on factors such as UV curing time, resolution, viscosity, and polymerization shrinkage [82].

Recently, an approach has been proposed in which the imprinted structure is directly used as an etching mask, avoiding the need for depositing separate etching masks [80]. In Figure 2c, a thin SU-8 photoresist layer is spin-coated and patterned via a soft mold to form an etching mask. Oxygen reactive ion etching (RIE) is used to remove the residual layer and further tune the mask dimensions both vertically and laterally, enabling control of nanopillar size during subsequent silicon etching. In this method, precise control of the etching process is essential, as insufficient etching leaves residual layers, while excessive etching leads to the formation of grass-like structures around nanostructure edges.

As such, although NIL offers a simpler fabrication route for metasurfaces as a replacement for the EBL method, the low refractive index of commercially available imprint resins makes their direct use as final meta-atoms challenging. Despite this limitation, an achromatic lens fabricated directly from a commercial imprint resin with a refractive index of ~1.5 are demonstrated in Figure 2d,e [81]. The metalenses have been successfully fabricated using Roll-to-Plate (R2P)-based NIL, involving the following steps: First, a high-resolution master mold is fabricated via high-speed EBL. A replica mold is then produced by coating the master mold with MINS-311RM resin and overlaying it with a flexible polyester film, followed by UV curing. Next, MINS-311RM resin is spin-coated onto a 4-inch glass substrate, which is gradually brought into contact with the replica mold to allow the resin to fill the nanostructures. Once full contact is achieved, the chamber is sealed under vacuum, and a uniform pressure of up to 19 kN is applied. The resin is rapidly cured under UV light, typically within one minute. Finally, the mold is separated. To enable high-throughput continuous patterning, the replica mold is rolled stepwise across the substrate, and a total of 16 achromatic metalenses are uniformly imprinted on each 4-inch wafer. Analysis of the metalens characteristics shows that the focal position deviation at 635 nm is 5.77 μm, which demonstrates its achromatic performance with nearly identical focal positions for red, green, and blue wavelengths. The focusing efficiencies are also measured to be 10.05%, 10.64%, and 9.51% at wavelengths of 450, 532, and 635 nm, respectively, indicating consistent performance across the spectral range. Despite the achromatic performance of metalenses, their efficiency remains limited because the low refractive index necessitates taller meta-atoms to achieve the required phase control. In large-scale mass production, however, the structure height cannot be increased beyond certain limits, underscoring the need for imprint resins with higher refractive indices to improve efficiency without compromising manufacturability.

2.3. Nanoimprint lithography for scalable metasurface fabrication

Despite the scalable, low-cost, and high-throughput advantages of the NIL process, its application in metasurface fabrication has been limited by the low refractive index (~1.5) of commercial imprint resins. Therefore, developing a high-index resin is crucial, as a sufficient optical path length is required to fully control the phase of light. In this chapter, we introduce two notable high-index NIL methods that are widely used in metasurface fabrication while maintaining the inherent benefits of NIL.

2.3.1. Hybrid material

The first approach to increasing the effective index of imprint resin is the use of a hybrid material, which involves coating an ALD film onto the imprinted metasurfaces [18]. Here, ALD enables conformal coating and the formation of high-index films, which can effectively confine light within the high-index layer, thereby increasing the effective index of metasurfaces. The overall procedure of hybrid approach is illustrated in Figure 3a–e. To begin with, a scalable master mold is fabricated using photolithography method. Photolithography is suitable for large-area fabrication, but it has been considered unsuitable for high-resolution applications since the resolution is proportional to source wavelength according to the Rayleigh criterion [83–86]. For instance, the resolution has been limited to ~400 nm for i-line steppers and ~200 nm for krypton fluoride (KrF) steppers. To address the resolution limitation, argon fluoride (ArF) excimer lasers are employed to achieve a resolution as low as 40 nm, suitable for metasurfaces spanning from infrared (IR) to UV [68,87]. Then, a resin-based soft mold is replicated from the master mold to ensure high process stability and suitability for repeated production. By using a soft mold as a stamp, metasurfaces can be repeatedly replicated onto the imprint resin under UV irradiation. Finally, to enhance the refractive index at a targeted wavelength, a conformal thin film is deposited via ALD process.

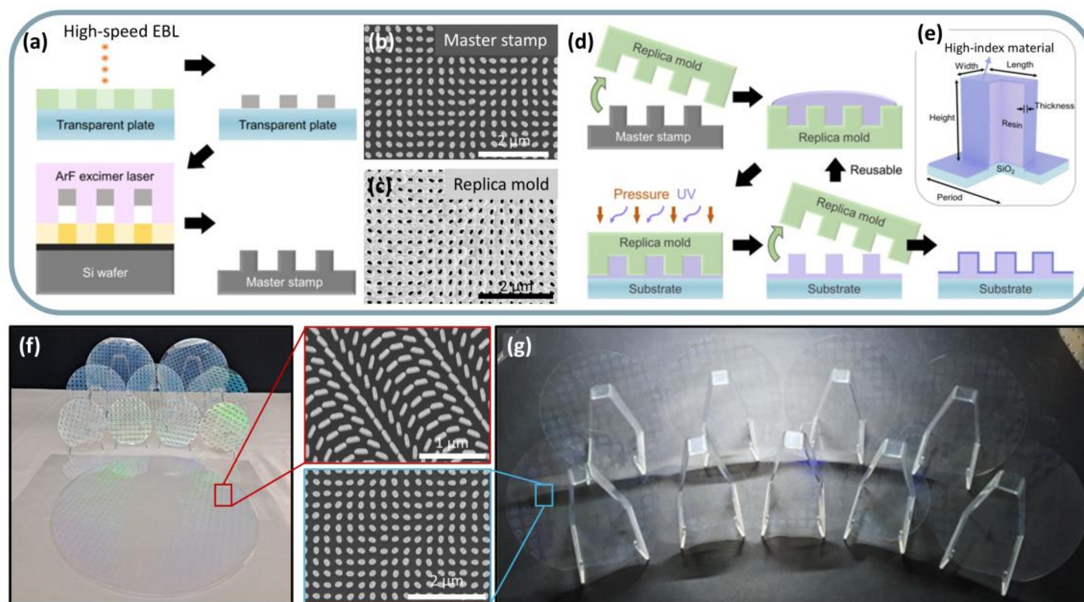

Figure 3. Fabrication of metasurfaces using hybrid material consisting of imprint resin and ALD layers. **(a, d)** Schematic illustration of NIL utilizing a hybrid material composed of imprint resin and ALD coatings; **(b)** SEM image of the fabricated master mold, and **(c)** the replicated soft mold; **(e)** Schematic diagram illustrating the geometrical parameters of the fabricated meta-atom [18]; **(f)** Photograph of the fabricated visible metalens formed by TiO_2 ALD coating on the imprinted metasurface [88]; **(g)** Photograph of the fabricated UV metalens formed by ZrO_2 coating on the imprinted metasurface [18].

Since the operating wavelength strongly depends on material properties, it can be readily tuned by depositing different materials. A representative example is the fabrication of a visible-range metalens by depositing a TiO_2 thin film via ALD (Figure 3f) [88]. Owing to its low optical loss and high refractive

index of approximately 2.3–2.5 in the visible range (450–635 nm), the TiO_2 thin film effectively enhances the effective index of the imprinted metalenses. The overall process is similar to that shown in Figure 3a–e, using tetrakis (dimethylamido) titanium (IV) (TDMAT) as the titanium precursor in plasma-enhanced ALD (PEALD). In PEALD, titanium precursor is oxidized by oxygen plasma, forming a TiO_2 thin film on the sample [89]. The thickness of the TiO_2 thin film is set to 23 nm, yielding maximum conversion efficiencies of 68.2% at 450 nm, 89.6% at 532 nm, and 79.7% at 635 nm. They also demonstrate the scalability of the hybrid method, achieving 1-cm visible metalenses fabricated on 4-, 6-, 8-, and 12-inch wafers. In addition, mass-produced metalenses are applied to a compact virtual reality (VR) prototype, using transmissive eyepieces to reduce the optical path and device volume. This demonstrates that NIL with hybrid materials can be integrated into practical VR systems while maintaining high performance.

In the UV range, maintaining low optical loss is particularly challenging because most high-index materials exhibit significant absorption. To address this, ZrO_2, with its wide bandgap of 6.195 eV, is selected for its low loss in the UV region. Furthermore, its high refractive index exceeding 2.2 across 250–400 nm makes it well suited for use in UV-range metalenses. Figure 3g shows UV metalenses with a diameter of 1 cm imprinted on 12-inch wafers using a ZrO_2-based hybrid material. Here, tetrakis (dimethylamino)zirconium (TDMAZr) is used as the zirconium precursor. The structure is designed with a 15 nm ALD layer and a meta-atom height of 550 nm, achieving a conversion efficiency of 80% at 325 nm. As a demonstration, they fabricate UV metalens using geometric phase control and verified their performance through simulations and experiments. The device achieves diffraction-limited focusing with an FWHM of ~1.2 μm and an average focusing efficiency of 45% across a 4-inch wafer, while imaging tests with a 1951 USAF target confirmed its high-resolution capability.

2.3.2. Particle-embedded resin

The other promising strategy is to incorporate high-index nanoparticles directly into the imprint resin [90–94]. By employing the PER process, metasurfaces can be fabricated in a single step, eliminating the need for additional refractive index enhancement and thereby simplifying fabrication [95]. The resin used in the PER-NIL process consists of nanoparticles, monomer, solvent, and UV or thermal initiator. The matrix resin, consisting of the monomer and initiator, functions as a crosslinker between nanoparticles, thereby influencing the transferability of metasurfaces. Also, since the refractive index of PER is strongly affected by nanoparticle concentration, both the resin and nanoparticle contents require precise optimization. The fabrication of conventional PER-NIL follows the steps illustrated in Figure 4a [65]. A master mold is first created using EBL, followed by the preparation of hard polydimethylsiloxane (h-PDMS). A thin, stiff h-PDMS layer is coated over the master mold to replicate the fine features, and a flexible PDMS buffer layer is subsequently coated to form a soft mold. This bilayer structure enables high-resolution pattern transfer, as the h-PDMS provides sufficient stiffness for accurate replication, while the underlying PDMS offers mechanical flexibility and reusability. PER is then spin-coated either onto the substrate or directly onto the soft mold. Patterning is achieved by applying appropriate pressure while heating or exposing the resin to UV light. Finally, careful detachment of the soft mold from the substrate leaves the imprinted metasurfaces on the substrate.

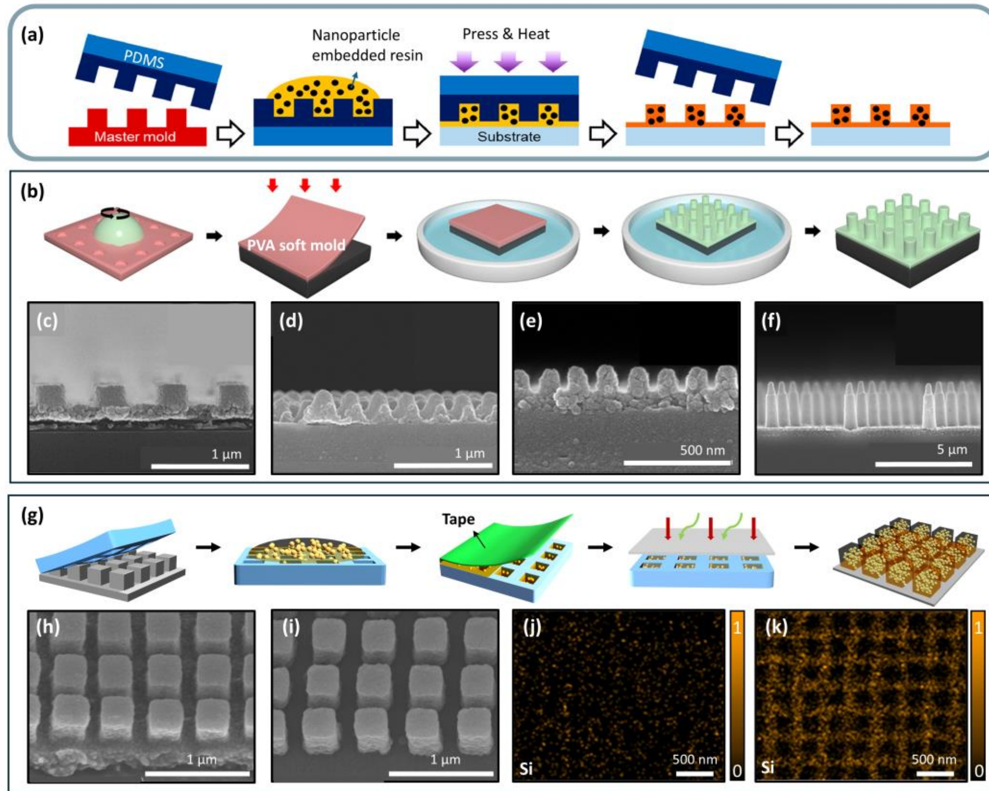

Figure 4. Fabrication of metasurfaces using particle-embedded resin (PER) consisting of matrix resin and nanoparticles. **(a)** The overall fabrication process of conventional PER-based NIL (PER-NIL) [65]. Reprinted with permission. Copyright 2021 American Chemical Society; **(b)** Nanoimprint lithography using a water-soluble polyvinyl alcohol (PVA) soft mold to enable demolding without shear stress. SEM images of various replicated structures include **(c)** nanopillars in a square array, **(d)** nano cones in a hexagonal array, **(e)** nano lines, and **(f)** high-aspect-ratio (HAR) pillar patterns (aspect ratio = 6) [96]; **(g)** Schematic illustration of the tape-assisted PER-NIL process for residual layer-free metasurfaces; **(h)** 15° tilted SEM image before residual layer removal **(i)** 15° tilted SEM image after residual layer removal. Energy-dispersive X-ray spectroscopy (EDS) analysis for Si showing **(j)** no Si signal from the substrate due to coverage by the residual layer (TiO_2), and **(k)** Si signal detected in region where the residual layer has been removed [97].

In PER-NIL process, high-aspect-ratio (HAR) structures are often required for full 2π phase coverage. However, during the physical demolding step, HAR structures are prone to damage due to the large shear stress exerted on the sidewalls. To overcome this limitation, a water-soluble polyvinyl alcohol (PVA) soft mold has been recently introduced as part of a NIL process in which the mold is dissolved in water (Figure 4b–f) [96]. The PVA soft mold, with its high tensile modulus of 2.936 MPa, is suitable for replicating metasurfaces with features below 100 nm. In addition, it removes the need for the vapor-phase self-assembled monolayer (SAM) coating process typically required for conventional h-PDMS molds to prevent pattern adhesion during demolding. Since PVA is a water-soluble polymer, the PVA mold covering the substrate dissolves in water, leaving only the replicated TiO_2 nanostructures on the substrate. Unlike conventional NIL, which introduces shear stress into cured nanostructures, the water-soluble mold demolding method used in this study enables defect-free replication. Using this

method, various nanostructures are fabricated with a PER composed of 30 nm TiO_2 nanoparticles. Since no shear stress is introduced during demolding, precise replication of nanopillars (Figure 4c), nano cones (Figure 4d), and nano lines (Figure 4e) are achieved, including HAR pillar patterns (Figure 4f) with an aspect ratio of 6. Furthermore, centimeter-scale HAR TiO_2 metalens arrays have been fabricated, achieving diffraction-limited focusing and a focusing efficiency of 28% at a wavelength of 532 nm.

Although PER-NIL enables one-step fabrication of metasurfaces, it has long been constrained by the high-index residual layer left on the substrate. The residual layer, composed of nanoparticles and matrix resin with different etching rates, cannot be fully removed by plasma etching and leads to optical losses such as reduced transmittance and light scattering. Here, a tape-assisted PER-NIL method has been developed to fabricate residual layer-free metasurfaces without the need for additional plasma etching [97]. This process is based on a high-index PER, composed of UV-curable resin uniformly dispersed with 60 wt% of TiO_2 nanoparticles (30 nm). The PER is first spin-coated onto a soft mold, and a polyethylene tape with optimized adhesion strength is then used to selectively peel off the residual layer without damaging the meta-atoms. Subsequently, UV curing is performed to enable clean transfer of the meta-atoms to the substrate (Figure 4g). To remove only the residual layer without damaging the meta-atoms, tape adhesion level is optimized. Excessive adhesion can partially peel off the meta-atoms along with the residual layer, whereas insufficient adhesion fails to remove the residual layer effectively. Through this optimization process, polyethylene tape is selected as the most suitable material. SEM and Energy-dispersive X-ray spectroscopy (EDS) analyses confirmed complete residual layer removal (Figure 4h–k). To demonstrate the optical potential of residual layer-free metasurfaces, structural color metasurfaces are fabricated. In such metasurfaces, a residual layer causes dual reflection peaks, while residual layer-free metasurfaces induce single-mode, high-purity reflection. The resulting residual layer-free metasurface exhibits a wide color gamut that nearly covers the entire sRGB space and demonstrates defect-free patterning of 3 × 3 arrays over an area of 1 cm^2, thereby proving the potential of tape-assisted PER-NIL. In addition, residual-free hologram metasurfaces exhibit improved transmittance of light and reduced light scattering, resulting in high-quality holograms with clearer images at 450, 532, and 635 nm.

2.3.3. Applications

PER offers the advantage of enabling the transfer of high-index materials without requiring additional deposition methods such as ALD or PECVD. Consequently, by simply changing the nanoparticle material in the PER solution, the transferred material and thus the operating wavelength can be easily modified. For instance, the incorporation of ZrO_2 [98], TiO_2 [97], and Si [65] nanoparticles enables coverage across the full spectral range from UV to visible and IR (Figure 5a–c). For UV metasurfaces, the fabrication of meta-atoms is particularly challenging because the required feature sizes scale down with the short operating wavelengths. To address this, efforts have been made to develop one-step printable approaches. Notably, the introduction of ZrO_2-based PER has enabled direct printing of UV metasurfaces. Owing to the high refractive index (~2.1) and low extinction coefficient of ZrO_2 nanoparticles across near- to deep-UV wavelengths, metaholograms operating at 325 nm and 248 nm have been successfully demonstrated. These devices achieve conversion efficiencies exceeding 70% and 48%, respectively, underscoring the practicality of this method for scalable UV optical systems (Figure 5a). For visible metasurfaces, which are central to a wide range of applications including

imaging and display technologies, single-step fabrication is particularly critical. In this spectral range, TiO_2 nanoparticles are employed due to their high refractive index (~1.94) and low extinction coefficient at visible wavelengths such as 532 nm. As shown in Figure 5b, structural color metasurfaces are realized using TiO_2-PER imprinting. These metasurfaces confine light strongly within the meta-atoms and selectively reflect specific wavelengths, thereby producing vivid coloration. By tuning the structural period and gap parameters for each color, simulation results reveal reflectance peaks at approximately 92%, 90%, and 88% for red (~635 nm), green (~532 nm), and blue (~450 nm) metasurfaces, respectively. Furthermore, optical microscopy images confirm that R, G, and B colors are experimentally reproduced at the corresponding wavelengths. Notably, by developing a residual layer-free imprinting process, the PER-based structural color metasurfaces achieve an expanded color gamut on the CIE 1931 chromaticity map, demonstrating their potential for high-fidelity color generation. IR metasurfaces enable compact and multifunctional imaging applications ranging from biomedical monitoring and 3D sensing to thermal cameras and gas detection. In Figure 5c, an IR metalens is fabricated using a Si nanoparticle-dispersed resin. Because Si strongly absorbs UV light due to its small bandgap, uniform curing is challenging in UV-NIL. Therefore, thermal NIL is employed to cure the Si-PER and realize high-index IR metalenses. The Si nanocomposite achieved a refractive index of ~2.2 across a broad spectral range (0.4–1 μm) with minimal shrinkage (~10%) after curing. Using this approach, metalenses with a diameter of 4 mm operating at 940 nm with 47% focusing efficiency are demonstrated. As a proof of concept, vein images beneath human skin are captured using the IR metalens integrated with a CMOS sensor, an adjustable aperture, and an NIR bandpass filter.

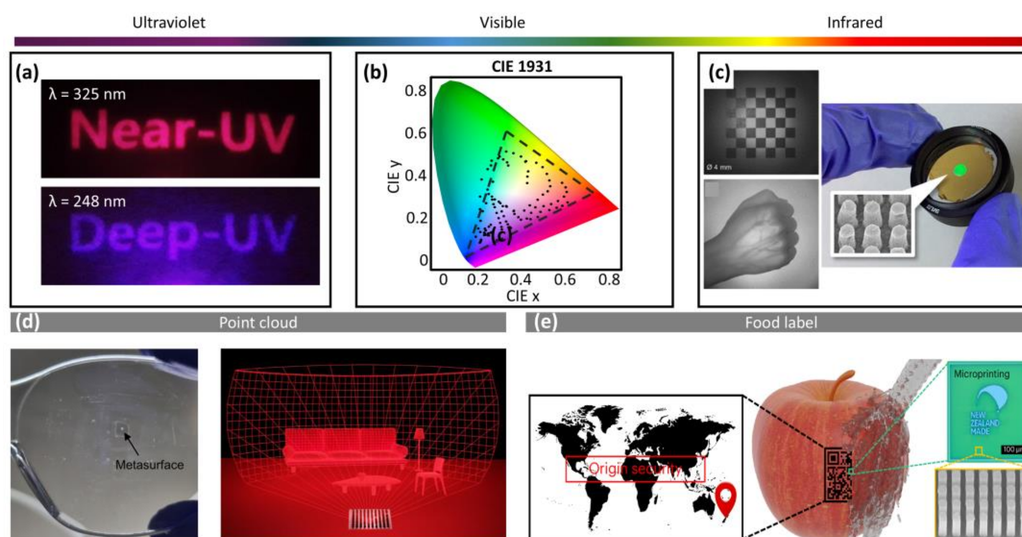

Figure 5. Broad applications of PER. **(a)** Holographic images in the UV range generated by a UV metasurface fabricated using a ZrO_2-PER [98]; **(b)** CIE 1931 chromaticity mapping of residual layer-free structural color metasurfaces in the visible range, fabricated using TiO_2-PER [97]; **(c)** Infrared (IR) metalens fabricated using Si-PER, with corresponding IR imaging results [65]. Reprinted with permission. Copyright 2021 American Chemical Society; **(d)** Metasurface-driven structured-light light detection and ranging (LiDAR) system. Left: metasurface transferred on curved surface of safety glass. Right: Concept schematic of metasurface-driven LiDAR system [99]; **(e)** Metasurface-based food label using biodegradable and water-soluble hydroxypropyl cellulose (HPC)-based TiO_2-PER [100].

Another notable advantage of PER is its ability to transfer metasurfaces onto curved surfaces, where conventional lithographic techniques are unable to achieve patterning. Patterning onto the curved surfaces provides significant advantages, enabling compact and lightweight optical systems for space-constrained applications such as mobile imaging, AR/VR headsets, and wearable sensors. Building on these advantages, metasurface-driven light detection and ranging (LiDAR) system is demonstrated using PER imprinting method [99]. The metasurface generates high-density (~1000) diffraction points over a full 180° field of view, enabling wide-angle and three-dimensional imaging. Crucially, metasurface for LiDAR system is directly transferred to the curved substrate, exemplified by safety-glass prototypes for compact AR depth sensors (Figure 5d). This study demonstrates the feasibility of PER-NIL integration into LiDAR systems and ergonomically suitable designs. Another notable example is the use of hydroxypropyl cellulose (HPC)-based PER in metasurface-enabled food labeling applications [100]. HPC is utilized for its biocompatible and water-soluble properties, enabling safe integration into food products [101]. Since it can be directly applied as a label on food and easily removed with water, it ensures no harm to the human body. In this work, TiO_2 nanoparticles are dispersed within an HPC matrix to produce a structural color-based label operating in the visible range. Importantly, these labels are successfully imprinted directly onto curved biological surfaces such as apples, demonstrating compatibility with non-planar food products and flexible packaging (Figure 5e).

3. Conclusion

In summary, this review covers the lithographic techniques for the fabrication of metasurfaces. We focus on NIL-based approaches that enable scalable and low-cost fabrication of metasurfaces. The progress in metasurface fabrication processes is summarized through three main chapters, and various applications enabled by scalable fabrication techniques are presented in the final section. To fabricate metasurfaces, EBL and PECVD have long been employed for high-resolution metasurface fabrication, but their slow throughput and high cost hinder scalable manufacturing. NIL has emerged as a low-cost, high-throughput alternative by replicating nanostructures with soft molds, yet its commercial resins suffer from low refractive indices that limit optical modulation. To overcome those limitations, two strategies have emerged: the use of hybrid materials and PERs. Hybrid materials use ALD coating after imprinting to raise the effective index, while PER mix high-index nanoparticles into the resin. Both approaches have successfully enabled scalable metasurface fabrication by overcoming the low-index limitation of commercial NIL resins, while maintaining the inherent advantages of high throughput and low cost. Depending on the purpose, desired feature sizes, and operating wavelengths, one of the two methods can be appropriately selected (Table 2).

Commercial interest in metasurfaces continues to rise, yet scalable fabrication has been hindered by the challenge of high-index materials and nanoscale patterning. To address this challenge, two NIL-based approaches can be considered. The first involves the use of hybrid material and PER strategies, as reviewed in this manuscript. Another promising direction is to combine NIL with other lithographic techniques. For instance, Damascene lithography [74,102], which is widely employed in dielectric metasurface fabrication, could be integrated with NIL. In such processes, NIL using photoresists [103,104] could serve as an alternative to the nanopatterning step in EBL, thereby enabling scalable, low-cost, and high-throughput manufacturing of metasurfaces. Further investigations into such

combined approaches could provide valuable insights and open new opportunities for advancing scalable metasurface fabrication.

Table 2. Comparison of hybrid materials and particle-embedded resin materials with respect to operating wavelengths, materials, and minimum feature sizes.

	Hybrid Material	Particle-Embedded Resin
UV region	ZrO_2 thin film	ZrO_2 nanoparticles
λ [reference]	350 nm [18]	248, 325 nm [95]
Visible region	TiO_2 thin film	TiO_2 nanoparticles
λ [reference]	450–635 nm [79]	450–635 nm [96]
IR region	-	Si nanoparticles
λ [reference]		940 nm [65]
Minimum feature size [reference]	60 nm [18]	60 nm [95]

4. Lessons learned

In this section, we share practical insights based on our firsthand experience with NIL using PER and hybrid material. Integrating PER and hybrid materials into NIL has shown strong potential for scalable metasurface manufacturing, but industrial-scale demonstrations are still lacking. To replace conventional diffractive optical elements, these processes must be combined with high-throughput methods such as roll-to-roll (R2R) or roll-to-plate (R2P). Here, we identify two main challenges:

(1) The high-index residual layer of PER can cause scattering and reduced transmittance of light, making it difficult to maintain consistent efficiency in mass-produced metasurfaces. Although our group has developed a tape-based removal method, further research is needed to assess its applicability to scalable fabrication.

(2) Temporal ALD, the most common ALD method, can hinder high-throughput processing because each cycle requires separate steps for precursor dosing, purging, and deposition. Therefore, alternative high-throughput ALD techniques are needed.

Commercializing metasurfaces could shift bulky optical systems toward compact, high-performance devices. Continued advances in fabrication will be essential, and we hope this review serves as a step in that direction.

In addition, for the industrial-scale implementation of NIL processes, it is essential to repeatedly use a single mold without damage or deformation, while ensuring accurate replication of the nanostructure patterns. To achieve this, specific materials [105] are coated onto the mold to reduce its surface energy, thereby decreasing the adhesion between the mold and the resin [106–108]. This is accomplished by coating the surface with self-assembled monolayers (SAM). The key requirement is that the SAM molecules must strongly adhere to the mold surface, while the opposite side which comes into contact with the resin should interact weakly to enable easy separation. When SAM coating is successfully performed, the surface energy decreases, resulting in a hydrophobic surface. Such surface treatment enhances the durability of the mold and enables stable demolding during repetitive imprinting processes, suggesting that further studies on surface treatment are still required.

Data availability statement

No new data were created or analyzed in this study. All data discussed in this review are sourced from previously published research, which is cited in the text.

Acknowledgements

This work was financially supported by the POSCO-POSTECH-RIST Convergence Research Center program funded by POSCO, the National Research Foundation (NRF) grants (RS-2025-25454431, RS-2024-00356928, RS-2024-00462912, RS-2024-00416272, RS-2024-00337012, RS-2024-00408286, RS-2022-NR067559, RS-2022-NR068141, RS-2022-NR068140) funded by the Ministry of Science and ICT (MSIT) of the Korean government, and Alchemist (No. 1415179744/20019169). Y.P. acknowledges the Presidential Science fellowship funded by the MSIT of the Korean government.

Authors' contribution

Conceptualization, J.R.; writing—original draft preparation, Y.P. and D.K.; writing—review and editing, Y.P. and D.K.; visualization, Y.P. and D.K.; supervision, J.R. All authors have read and agreed to the published version of the manuscript.

Conflicts of interests

Junsuk Rho holds the position of Associate Editor-in-chief for *Optics and Photonics Research* and has not peer reviewed or made any editorial decisions for this paper.

References

[1] Kim J, Jeon D, Seong J, Badloe T, Jeon N, *et al.* Photonic encryption platform via dual-band vectorial metaholograms in the ultraviolet and visible. *ACS Nano* 2022, 16(3):3546–3553.

[2] Park C, Jeon Y, Rho J. 36-channel spin and wavelength co-multiplexed metasurface holography by phase-gradient inverse design. *Adv. Sci.* 2025, 12(28):2504634.

[3] Noh J, Kim J, Rho J. Overcoming information sparsity in metasurfaces for full-color holography via end-to-end design. *Nano Lett.* 2025, 25(29):11398–11405.

[4] Park C, Lee E, Kim J, Kim W, Song H, *et al.* 12″ Wafer-scale mass-manufactured metal–insulator–metal reflective metaholograms by nanotransfer printing. *ACS Appl. Mater. Interfaces* 2025, 17(2):3749–3756.

[5] Asad A, Seong J, Khaliq HS, Lee JW, Jeon Y, *et al.* Wide-angled pragmatic dielectric chiral meta-platform for spin- and wavelength-multiplexed holography in the ultraviolet and visible. *Adv. Funct. Mater.* 2024, 34(41):2402744.

[6] Yu G, Mao X, Ding H, Yang F, Wang X. Inverse-designed polarization-insensitive metasurface holography fabricated by nanoimprint lithography. *Opt. Lett.* 2024, 49(23):6845–6848.

[7] Kim J, Jeong M, Jung C, Seong J, Rho J. Electro-active metasurfaces controlling exceptional topological phase through low-voltage operation on conductive polymer. *Adv. Funct. Mater.* 2025, 35(38):2501916.

[8] Gong J, Xiong L, Pu M, Li X, Ma X, *et al.* Visible meta-displays for anti-counterfeiting with printable dielectric metasurfaces. *Adv. Sci.* 2024, 11(17):2308687.

[9] Fan Y, Liang H, Wang Y, Chen S, Lai F, *et al.* Dual-channel quantum meta-hologram for display. *Adv. Photonics Nexus* 2024, 3(1):016011.

[10] Lee C, Lee S, Seong J, Park DY, Rho J. Inverse-designed metasurfaces for highly saturated transmissive colors. *J. Opt. Soc. Am. B* 2024, 41(1):151–158.

[11] Jang J, Badloe T, Yang Y, Lee T, Mun J, *et al.* Spectral modulation through the hybridization of mie-scatterers and quasi-guided mode resonances: realizing full and gradients of structural color. *ACS Nano* 2020, 14(11):15317–15326.

[12] Jang J, Badloe T, Sim YC, Yang Y, Mun J, *et al.* Full and gradient structural colouration by lattice amplified gallium nitride Mie-resonators. *Nanoscale* 2020, 12(41):21392–21400.

[13] Kim I, Yun J, Badloe T, Park H, Seo T, *et al.* Structural color switching with a doped indium-gallium-zinc-oxide semiconductor. *Photon. Res.* 2020, 8(9):1409–1415.

[14] Sun S, Zhou Z, Zhang C, Gao Y, Duan Z, *et al.* All-dielectric full-color printing with TiO2 metasurfaces. *ACS Nano* 2017, 11(5):4445–4452.

[15] Zhu X, Yan W, Levy U, Mortensen NA, Kristensen A. Resonant laser printing of structural colors on high-index dielectric metasurfaces. *Sci. Adv.* 2017, 3(5):e1602487.

[16] Koirala I, Lee SS, Choi DY. Highly transmissive subtractive color filters based on an all-dielectric metasurface incorporating TiO2 nanopillars. *Opt. Express* 2018, 26(14):18320–18330.

[17] Song M, Feng L, Huo P, Liu M, Huang C, *et al.* Versatile full-colour nanopainting enabled by a pixelated plasmonic metasurface. *Nat. Nanotechnol.* 2023, 18(1):71–78.

[18] Kim J, Kim Y, Kim W, Oh DK, Kang D, *et al.* 8″ wafer-scale, centimeter-sized, high-efficiency metalenses in the ultraviolet. *Mater. Today* 2024, 73:9–15.

[19] Badloe T, Kim I, Kim Y, Kim J, Rho J. Electrically tunable bifocal metalens with diffraction-limited focusing and imaging at visible wavelengths. *Adv. Sci.* 2021, 8(21):2102646.

[20] Barulin A, Kim Y, Oh DK, Jang J, Park H, *et al.* Dual-wavelength metalens enables Epi-fluorescence detection from single molecules. *Nat. Commun.* 2024, 15(1):26.

[21] Badloe T, Seong J, Rho J. Trichannel spin-selective metalenses. *Nano Lett.* 2023, 23(15):6958–6965.

[22] Kim Y, Lee J, Yeo WH, Li X, Kim WS, *et al.* Rapid polarization-controlled depth sensing and imaging with an electrically tunable metalens. *Nano Lett.* 2025, 25(23):9394–9401.

[23] Khorasaninejad M, Capasso F. Metalenses: versatile multifunctional photonic components. *Science* 2017, 358(6367):eaam8100.

[24] Yun JG, Kang H, Lee K, Jeong Y, Lee E, *et al.* Compact eye camera with two-third wavelength phase-delay metalens. *Nat. Commun.* 2025, 16(1):7299.

[25] Tang P, Jeon Y, Li X, Kim Y, Seong J, *et al.* Switchable bright-field imaging and corner detection with an electrically tunable metalens. *Adv. Opt. Mater.* 2025, 13(22):2500981.

[26] McClung A, Torfeh M, Einck VJ, Watkins JJ, Arbabi A. Visible metalenses with high focusing efficiency fabricated using nanoimprint lithography. *Adv. Opt. Mater.* 2024, 12(9):2301865.

[27] Park JS, Lim SWD, Amirzhan A, Kang H, Karrfalt K, *et al.* All-glass 100 mm diameter visible metalens for imaging the cosmos. *ACS Nano* 2024, 18(4):3187–3198.

[28] Xiong J, Hsiang EL, He Z, Zhan T, Wu ST. Augmented reality and virtual reality displays: emerging technologies and future perspectives. *Light Sci. Appl.* 2021, 10(1):216.

[29] Song Y, Yuan J, Chen Q, Liu X, Zhou Y, *et al.* Three-dimensional varifocal meta-device for augmented reality display. *PhotoniX* 2025, 6(1):6.

[30] Gan Y, Xiao J, Plaskocinski T, Persheyev S, Biabanifard M, *et al.* See-through conformable holographic metasurface patches for augmented reality. *Laser Photonics Rev.* 2025, 19(4):2401240.
[31] Lee GY, Hong JY, Hwang S, Moon S, Kang H, *et al.* Metasurface eyepiece for augmented reality. *Nat. Commun.* 2018, 9(1):4562.
[32] Kim I, Kim H, Go M, Lee S, Nguyen DD, *et al.* Ultrafast metaphotonic PCR chip with near-perfect absorber. *Adv. Mater.* 2024, 36(39):2311931.
[33] Altug H, Oh SH, Maier SA, Homola J. Advances and applications of nanophotonic biosensors. *Nat. Nanotechnol.* 2022, 17(1):5–16.
[34] Tseng ML, Jahani Y, Leitis A, Altug H. Dielectric metasurfaces enabling advanced optical biosensors. *ACS Photonics* 2021, 8(1):47–60.
[35] Kim H, Yun H, Jeong S, Lee S, Cho E, *et al.* Optical metasurfaces for biomedical imaging and sensing. *ACS Nano* 2025, 19(3):3085–3114.
[36] Talts ÜL, Weigand H, Occhiodori I, Grange R. Scalable lithium niobate nanoimprinting for nonlinear metalenses. *Adv. Mater.* 2025, 37(27):2418957.
[37] Barulin A, Barulina E, Oh DK, Jo Y, Park H, *et al.* Axially multifocal metalens for 3D volumetric photoacoustic imaging of neuromelanin in live brain organoid. *Sci. Adv.* 2025, 11(3):eadr0654.
[38] Kim S, Kim J, Kim K, Jeong M, Rho J. Anti-aliased metasurfaces beyond the Nyquist limit. *Nat. Commun.* 2025, 16(1):411.
[39] Badloe T, Yang Y, Lee S, Jeon D, Youn J, *et al.* Artificial intelligence-enhanced metasurfaces for instantaneous measurements of dispersive refractive index. *Adv. Sci.* 2024, 11(39):2403143.
[40] Lee D, Oh B, Park J, Moon SW, Shin K, *et al.* Wide field-of-hearing metalens for aberration-free sound capture. *Nat. Commun.* 2024, 15(1):3044.
[41] Ijaz S, Kang D, Rana AS, Kim J, Chani MTS, *et al.* Metasurface absorber–emitter pair-integrated high-efficiency thermophotovoltaic system. *ACS Photonics* 2025, 12(7):3829–3839.
[42] Shafqat MD, Park Y, Mahmood N, Kim J, Kang D, *et al.* dual-band metasurface-based structured light generations for futuristic communication applications. *Small Sci.* 2025, 5(5):2400524.
[43] Babicheva VE, Chang CC. Atomic layer deposition for enhanced light confinement in nonlinear metasurfaces. *ACS Omega* 2025, 10(22):23150–23160.
[44] Chou SY, Krauss PR, Renstrom PJ. Imprint of sub-25 nm vias and trenches in polymers. *Appl. Phys. Lett.* 1995, 67(21):3114–3116.
[45] Hirai Y, Yoshida S, Takagi N. Defect analysis in thermal nanoimprint lithography. *J. Vac. Sci. Technol. B* 2003, 21(6):2765–2770.
[46] Chen S, Chen H, Gao Y, Chen X, Hao Z, *et al.* Fabrication of slanted gratings with high refractive index starting from master nanoimprint mold. *Opt. Express* 2024, 32(23):40886–40897.
[47] Guo LJ. Nanoimprint lithography: methods and material requirements. *Adv. Mater.* 2007, 19(4):495–513.
[48] Khang DY, Kang H, Kim TI, Lee HH. Low-pressure nanoimprint lithography. *Nano Lett.* 2004, 4(4):633–637.
[49] Fan Y, Wang C, Tian H, Chen X, Li B, *et al.* Electric-field-driven generative nanoimprinting for tilted metasurface nanostructures. *Nano Micro Lett.* 2025, 18(1):12.
[50] Chen Y. Applications of nanoimprint lithography/hot embossing: a review. *Appl. Phys. A* 2015, 121(2):451–465.

[51] Park S, Song Z, Brumfield L, Amirsadeghi A, Lee J. Demolding temperature in thermal nanoimprint lithography. *Appl. Phys. A* 2009, 97(2):395–402.

[52] Modaresialam M, Chehadi Z, Bottein T, Abbarchi M, Grosso D. Nanoimprint lithography processing of inorganic-based materials. *Chem. Mater.* 2021, 33(14):5464–5482.

[53] Alnakhli Z, Liu Z, AlQatari F, Cao H, Li X. UV-assisted nanoimprint lithography: the impact of the loading effect in silicon on nanoscale patterns of metalens. *Nanoscale Adv.* 2024, 6(11):2954–2967.

[54] Pelloquin S, Augé S, Sharshavina K, Doucet JB, Héliot A, *et al.* Soft mold nanoimprint lithography: a versatile tool for sub-wavelength grating applications. *Microsyst. Technol.* 2022, 28(6):1293–1300.

[55] Yoon G, Kim K, Huh D, Lee H, Rho J. Single-step manufacturing of hierarchical dielectric metalens in the visible. *Nat. Commun.* 2020, 11(1):2268.

[56] Einck VJ, Torfeh M, McClung A, Jung DE, Mansouree M, *et al.* Scalable nanoimprint lithography process for manufacturing visible metasurfaces composed of high aspect ratio TiO2 meta-atoms. *ACS Photonics* 2021, 8(8):2400–2409.

[57] Kim J, Oh DK, Kim H, Yoon G, Jung C, *et al.* Metasurface holography reaching the highest efficiency limit in the visible via one-step nanoparticle-embedded-resin printing. *Laser Photonics Rev.* 2022, 16(8):2200098.

[58] Kang H, Kim H, Kim K, Rho J. Printable spin-multiplexed metasurfaces for ultraviolet holographic displays. *ACS Nano* 2024, 18(32):21504–21511.

[59] Kim I, Kim WS, Kim K, Ansari MA, Mehmood MQ, *et al.* Holographic metasurface gas sensors for instantaneous visual alarms. *Sci. Adv.* 2021, 7(15):eabe9943.

[60] Naveed MA, Kim J, Ansari MA, Kim I, Massoud Y, *et al.* Single-step fabricable flexible metadisplays for sensitive chemical/biomedical packaging security and beyond. *ACS Appl. Mater. Interfaces* 2022, 14(27):31194–31202.

[61] Kim K, Yoon G, Baek S, Rho J, Lee H. Facile nanocasting of dielectric metasurfaces with sub-100 nm resolution. *ACS Appl. Mater. Interfaces* 2019, 11(29):26109–26115.

[62] Moon SW, Kim J, Park C, Kim W, Yang Y, *et al.* Wafer-scale manufacturing of near-infrared metalenses. *Laser Photonics Rev.* 2024, 18(4):2300929.

[63] So S, Kim J, Badloe T, Lee C, Yang Y, *et al.* Multicolor and 3D holography generated by inverse-designed single-cell metasurfaces. *Adv. Mater.* 2023, 35(17):2208520.

[64] Kim W, Yoon G, Kim J, Jeong H, Kim Y, *et al.* Thermally-curable nanocomposite printing for the scalable manufacturing of dielectric metasurfaces. *Microsyst. Nanoeng.* 2022, 8(1):73.

[65] Yoon G, Kim K, Kim SU, Han S, Lee H, *et al.* Printable nanocomposite metalens for high-contrast near-infrared imaging. *ACS Nano* 2021, 15(1):698–706.

[66] Park C, Kim W, Kim Y, Sung H, Park J, *et al.* High-throughput fabrication of large-scale metaholograms via one-step printing. *Adv. Opt. Mater.* 2024, 12(9):2301562.

[67] Yang Y, Yoon G, Park S, Namgung SD, Badloe T, *et al.* Revealing structural disorder in hydrogenated amorphous silicon for a low-loss photonic platform at visible frequencies. *Adv. Mater.* 2021, 33(9):2005893.

[68] Li N, Fu Y, Dong Y, Hu T, Xu Z, *et al.* Large-area pixelated metasurface beam deflector on a 12-inch glass wafer for random point generation. *Nanophotonics* 2019, 8(10):1855–1861.

[69] Yeh TW, Hung YH, Chung CS, Yeh SJ, Lee HY, *et al.* Nanotransfer printed dual-layer metasurfaces for infrared cut-off applications. *ACS Appl. Nano Mater.* 2024, 7(22):25593–25602.

[70] Kooy N, Mohamed K, Pin LT, Guan OS. A review of roll-to-roll nanoimprint lithography. *Nanoscale Res. Lett.* 2014, 9(1):320.

[71] Jeong M, Lee J, Kim S, Gong X, Fang R, *et al.* Obtuse-angled separation of chiral resonances with planar asymmetry–induced tunability of quality factors. *Sci. Adv.* 2025, 11(30):eadu4875.

[72] Lee J, Jeong M, Jang J, Kim J, Mun J, *et al.* Bound-states-in-the-continuum-induced directional photoluminescence with polarization singularity in WS2 monolayers. *Nano Lett.* 2025, 25(2):861–867.

[73] Moon S, Kim S, Kim J, Lee CK, Rho J. Single-layer waveguide displays using achromatic metagratings for full-colour augmented reality. *Nat. Nanotechnol.* 2025, 20(6):747–754.

[74] Dorrah AH, Park JS, Palmieri A, Capasso F. Free-standing bilayer metasurfaces in the visible. *Nat. Commun.* 2025, 16(1):3126.

[75] Liu N, Tang ML, Hentschel M, Giessen H, Alivisatos AP. Nanoantenna-enhanced gas sensing in a single tailored nanofocus. *Nat. Mater.* 2011, 10(8):631–636.

[76] Kim I, Jeong H, Kim J, Yang Y, Lee D, *et al.* Dual-band operating metaholograms with heterogeneous meta-atoms in the visible and near-infrared. *Adv. Opt. Mater.* 2021, 9(19):2100609.

[77] Liu N, Hentschel M, Weiss T, Alivisatos AP, Giessen H. Three-dimensional plasmon rulers. *Science* 2011, 332(6036):1407–1410.

[78] Stolt T, Kim J, Héron S, Vesala A, Yang Y, *et al.* Backward phase-matched second-harmonic generation from stacked metasurfaces. *Phys. Rev. Lett.* 2021, 126(3):033901.

[79] Gong J, Xiong L, Pu M, Guo Y, Wen Y, *et al.* Simple route for high-throughput fabrication of metasurfaces using one-step UV-curable resin printing. *Opt. Express* 2023, 31(5):8068–8080.

[80] Cao X, Xiao Y, Dong Q, Zhang S, Wang J, *et al.* Tuning metasurface dimensions by soft nanoimprint lithography and reactive ion etching. *Adv. Photonics Res.* 2022, 3(11):2200127.

[81] Choi M, Kim J, Moon S, Shin K, Nam SW, *et al.* Roll-to-plate printable RGB achromatic metalens for wide-field-of-view holographic near-eye displays. *Nat. Mater.* 2025, 24(4):535–543.

[82] Vogler M, Wiedenberg S, Mühlberger M, Bergmair I, Glinsner T, *et al.* Development of a novel, low-viscosity UV-curable polymer system for UV-nanoimprint lithography. *Microelectron. Eng.* 2007, 84(5):984–988.

[83] She A, Zhang S, Shian S, Clarke DR, Capasso F. Large area metalenses: design, characterization, and mass manufacturing. *Opt. Express* 2018, 26(2):1573–1585.

[84] Tao J, You Q, Li Z, Luo M, Liu Z, *et al.* Mass-manufactured beam-steering metasurfaces for high-speed full-duplex optical wireless-broadcasting communications. *Adv. Mater.* 2022, 34(6):2106080.

[85] Leitis A, Tseng ML, John-Herpin A, Kivshar YS, Altug H. Wafer-scale functional metasurfaces for mid-infrared photonics and biosensing. *Adv. Mater.* 2021, 33(43):2102232.

[86] Park JS, Zhang S, She A, Chen WT, Lin P, *et al.* All-glass, large metalens at visible wavelength using deep-ultraviolet projection lithography. *Nano Lett.* 2019, 19(12):8673–8682.

[87] Hu T, Tseng CK, Fu Y, Xu Z, Dong Y, *et al.* Demonstration of color display metasurfaces via immersion lithography on a 12-inch silicon wafer. *Opt. Express* 2018, 26(15):19548–19554.

[88] Kim J, Seong J, Kim W, Lee GY, Kim S, *et al.* Scalable manufacturing of high-index atomic layer–polymer hybrid metasurfaces for metaphotonics in the visible. *Nat. Mater.* 2023, 22(4):474–481.
[89] Schindler P, Logar M, Provine J, Prinz FB. Enhanced step coverage of TiO2 deposited on high aspect ratio surfaces by plasma-enhanced atomic layer deposition. *Langmuir* 2015, 31(18):5057–5062.
[90] Jo HB, Byeon KJ, Lee H, Kwon MH, Choi KW. Fabrication of ZnO nano-structures using UV nanoimprint lithography of a ZnO nano-particle dispersion resin. *J. Mater. Chem.* 2012, 22(38):20742–20746.
[91] Choi JH, Jo HB, Choi HJ, Lee H. Fabrication of TiO2 nano-to-microscale structures using UV nanoimprint lithography. *Nanotechnology* 2013, 24(19):195301.
[92] Zhang C, Divitt S, Fan Q, Zhu W, Agrawal A, *et al.* Low-loss metasurface optics down to the deep ultraviolet region. *Light Sci. Appl.* 2020, 9(1):55.
[93] Zhang C, Chen L, Lin Z, Song J, Wang D, *et al.* Tantalum pentoxide: a new material platform for high-performance dielectric metasurface optics in the ultraviolet and visible region. *Light Sci. Appl.* 2024, 13(1):23.
[94] Huang K, Deng J, Leong HS, Yap SLK, Yang RB, *et al.* Ultraviolet metasurfaces of ≈ 80% efficiency with antiferromagnetic resonances for optical vectorial anti-counterfeiting. *Laser Photonics Rev.* 2019, 13(5):1800289.
[95] Jeong M, Ko B, Jung C, Kim J, Jang J, *et al.* Printable light-emitting metasurfaces with enhanced directional photoluminescence. *Nano Lett.* 2024, 24(19):5783–5790.
[96] Choi H, Kim J, Kim W, Seong J, Park C, *et al.* Realization of high aspect ratio metalenses by facile nanoimprint lithography using water-soluble stamps. *PhotoniX* 2023, 4(1):18.
[97] Park Y, Kim J, Yang Y, Oh DK, Kang H, *et al.* Tape-assisted residual layer-free one-step nanoimprinting of high-index hybrid polymer for optical loss-suppressed metasurfaces. *Adv. Sci.* 2025, 12(10):2409371.
[98] Kim J, Kim W, Oh DK, Kang H, Kim H, *et al.* One-step printable platform for high-efficiency metasurfaces down to the deep-ultraviolet region. *Light Sci. Appl.* 2023, 12(1):68.
[99] Kim G, Kim Y, Yun J, Moon SW, Kim S, *et al.* Metasurface-driven full-space structured light for three-dimensional imaging. *Nat. Commun.* 2022, 13(1):5920.
[100] Kim J, Kim H, Kang H, Kim W, Chen Y, *et al.* A water-soluble label for food products prevents packaging waste and counterfeiting. *Nat. Food* 2024, 5(4):293–300.
[101] Espinha A, Dore C, Matricardi C, Alonso MI, Goñi AR, *et al.* Hydroxypropyl cellulose photonic architectures by soft nanoimprinting lithography. *Nat. Photonics* 2018, 12(6):343–348.
[102] Chen WT, Park JS, Marchioni J, Millay S, Yousef KMA, *et al.* Dispersion-engineered metasurfaces reaching broadband 90% relative diffraction efficiency. *Nat. Commun.* 2023, 14(1):2544.
[103] Wang J, Zhao Y, Agha I, Sarangan AM. SU-8 nanoimprint fabrication of wire-grid polarizers using deep-UV interference lithography. *Opt. Lett.* 2015, 40(19):4396–4399.
[104] Hauser H, Herter B, Hofmann CLM, Höhn O, Kübler V, *et al.* Soft thermal nanoimprint of PMMA doped with upconverter nanoparticles. *Microelectron. Eng.* 2018, 187–188:154–159.
[105] Ulman A. Formation and structure of self-assembled monolayers. *Chem. Rev.* 1996, 96(4):1533–1554.
[106] Jung GY, Li Z, Wu W, Chen Y, Olynick DL, *et al.* Vapor-phase self-assembled monolayer for improved mold release in nanoimprint lithography. *Langmuir* 2005, 21(4):1158–1161.

[107] Liu N, Sun L, Jin P, Lin J, Tan J. Temperature effect of vapor-phase self-assembled monolayer for anti-sticking layers used in UV-embossing. In *2013 International Conference on Manipulation, Manufacturing and Measurement on the Nanoscale*, Suzhou, China, August 26–30, 2013, pp. 353–356.

[108] Steinberg C, Dhima K, Blenskens D, Mayer A, Wang S, *et al*. A scalable anti-sticking layer process via controlled evaporation. *Microelectron. Eng.* 2014, 123:4–8.